Novel *SCN9A* missense mutations contribute to congenital insensitivity to pain: Unexpected correlation between electrophysiological characterization and clinical phenotype

Jiaoli Sun[1] Lulu Li[2] Luyao Yang[2], Guangyou Duan[1,3], Tingbin Ma[2], Ningbo Li[1], Yi Liu[1], Jing Yao[4], Jing Yu Liu[2], and Xianwei Zhang[1]

Abstract

Congenital insensitivity to pain (OMIM 243000) is an extremely rare disorder caused by loss-of-function mutations in *SCN9A* encoding Nav1.7. Although the *SCN9A* mutations and phenotypes of painlessness and anosmia/hyposmia in patients are previously well documented, the complex relationship between genotype and phenotype of congenital insensitivity to pain remains unclear. Here, we report a congenital insensitivity to pain patient with novel *SCN9A* mutations. Functional significance of novel *SCN9A* mutations was assessed in HEK293 cells expressing Nav1.7, the results showed that p.Arg99His significantly decreased current density and reduced total Nav1.7 protein levels, whereas p.Trp917Gly almost abolished Nav1.7 sodium current without affecting its protein expression. These revealed that mutations in Nav1.7 in this congenital insensitivity to pain patient still retained partial channel function, but the patient showed completely painlessness, the unexpected genotypic-phenotypic relationship of *SCN9A* mutations in our patient may challenge the previous findings "Nav1.7 total loss-of-function leads to painlessness." Additionally, these findings are helpful for understanding the critical amino acid for maintaining function of Nav1.7, thus contributing to the development of Nav1.7-targeted analgesics.

Introduction

Congenital insensitivity to pain (CIP) (OMIM 243000), an extremely rare autosomal recessively inherited disorder, is characterized by lack of pain-related protective mechanisms against noxious stimuli, which predisposes patients to self-mutilations, burns, and painless fractures. In addition, CIP patients may also experience anosmia or hyposmia. CIP is caused by loss-of-function mutations in *SCN9A* located on chromosome 2 (2q24.3),[1] which contains 27 exons and encodes the subunit of sodium channel isoform Nav1.7. The channel shares structural similarity with other mammalian voltage-gated sodium channel subtypes (Nav1.1 to Nav1.6, Nav1.8, and Nav1.9), which are composed of

[1]Department of Anesthesiology, Tongji Hospital, Tongji Medical College, Huazhong University of Science and Technology, Wuhan, People's Republic of China
[2]Key Laboratory of Molecular Biophysics of the Ministry of Education, College of Life Science and Technology and Center for Human Genome Research, Huazhong University of Science and Technology, Wuhan, People's Republic of China
[3]Department of Anesthesiology, The Second Affiliated Hospital, Chongqing Medical University, Chongqing, People's Republic of China
[4]College of Life Sciences, Wuhan University, Wuhan, People's Republic of China

The first two authors contributed equally to this work.

Corresponding Authors:
Xianwei Zhang, Department of Anesthesiology, Tongji Hospital, Tongji Medical College, Huazhong University of Science and Technology, No. 1095 Jie-Fang Road, Wuhan 430030, People's Republic of China.
Email: ourpain@163.com
Jing Yu Liu, Center for Human Genome Research, College of Life Science and Technology, 1037 Luoyu Road, Wuhan 430074, People's Republic of China.
Email: liujy@mail.hust.edu.cn

four homologous domains (DI−DIV) with each containing six transmembrane segments (S1−S6), connected by intracellular loops (L1, L2, and L3) and cytoplasmic N- and C-terminal regions.[2,3] Segments S1–S4 are involved in voltage sensing, whereas S5 and S6 folded into the sodium ion pore are critical for selective permeation of sodium ions.[4]

To date, only 37 *SCN9A* mutations have been implicated in CIP in the worldwide. Moreover, most of the *SCN9A* mutations identified in CIP patients are mainly frame-shift, nonsense, and splicing mutations, all of which produced non-functional and truncated Nav1.7 proteins[5] (Figure S1). However, missense mutations in *SCN9A* causing CIP are extremely rare and the complex relationship between genotype and phenotype remains unclear.

Here, we identify *SCN9A* mutations in a Chinese Han girl suffering from insensitivity to pain. The functional significance of novel *SCN9A* mutations was explored using HEK293 cells expressing Nav1.7, and the Nav1.7 levels were analyzed by polymerase chain reaction (PCR), Western blotting, and immunocytochemistry, and electrophysiological activity was detected by whole-cell patch clamp recording.

Materials and methods

Ethics

The study was approved by the ethical committee of Tongji Hospital, Huazhong University of Science and Technology (approval no. 20130501) and was conducted following the guidelines of the Declaration of Helsinki. Written informed consent was obtained from the participants before the study.

Subjects and their phenotypes

A child with insensitivity to pain and her parents participated in our study. The proband, a 2.5-year-old girl with CIP from Harbin, China, was the only daughter of non-consanguineous parents who were normal during pregnancy and childbirth (Figure 1(a)). There was no history of neurological disease in the family.

The medical history of patient's insensitivity to pain was reconstructed by a questionnaire related to CIP symptoms, after that, the patient and her parents were invited to interview, and physical examinations were carried out to confirm the diagnosis.

Mutation analysis

Peripheral blood samples were collected from the elbow vein, and the genomic DNA was extracted using the guanidinium isothiocyanate method. The genomic DNA of the proband was sent to the Beijing Genomics Institute for gene sequencing using the GeneChip Technology, and the detected genes included 60 pain-related genes, such as *SCN9A*, *SCN10A*, *NGF*, *NTRK1*, and *PRDM12*.

Construction of Nav1.7 expression plasmids

The cDNA of human Nav1.7 (NM_002977.3) was subcloned into the pcDNA3.1mod vector,[6] and mutations (c.296G>A, p.Arg99His and c.2749T>G, p.Trp917Gly) (referred to as R99H and W917G, respectively, in the figures) were introduced using overlap extension PCR with primers and verified by Sanger sequencing.

Culture and transfection of HEK293 cells

Human embryonic kidney (HEK293) cells were plated in 3.5-cm plastic dishes (NEST) in Dulbecco's Modified Eagle Medium (Gibco) supplemented with 10% fetal bovine serum (Gibco) and 1% penicillin (100 U/ml)/streptomycin (100 μg/ml) (HyClone) and grown at standard conditions (37°C, 5% CO_2) for about 12 h. Then, cells were co-transfected with wild-type (WT) or mutant *SCN9A* constructs (1.5 μg each) and *EGFP* (0.15 μg) using the PolyJet transfection reagent (SignaGen) according to the manufacturer's instructions and incubated for 24 h.

Electrophysiological analysis

Transfected cells were collected, resuspended in 1 ml culture medium, diluted 1:15, seeded onto poly-L-lysine coated glass cover slips, and used for electrophysiological analysis within 10 h. EGFP-labeled HEK293 cells were selected for whole-cell patch clamp recording performed using an Axopatch 200B amplifier and the custom-designed Exclamp software at room temperature ($22 \pm 1°C$). Extracellular bath solution contained (mM): 140 NaCl, 5 KCl, 2 $CaCl_2$, 10 HEPES, 0.1 $CdCl_2$, 20 TEA-Cl, 0.001 TTX, and 10–30 glucose (pH 7.4 adjusted with NaOH). Pipette solution contained (mM):135 CsF, 10 NaCl, 2.5 $MgCl_2$, 10 HEPES, 1 EGTA, 5 TEA-Cl, and 4 Mg-ATP (pH 7.4 adjusted with CsOH). In the study, osmolarity of the recording and bath solutions is adjusted to 320 mOsm for extracellular solution and 310 mOsm for intracellular solution.

Fire-polished electrodes were fabricated from borosilicate glass (VitalSense Scientific Instruments Co., Ltd., China) using P-97 pipette puller (Sutter Instrument), and they had a resistance below 3 MΩ when filled with the pipette solution. HEK293 cells were held at −120 mV in all experiments.

Pipette potential was adjusted to zero before seal formation and 80%–90% series resistance compensation was applied to reduce voltage errors. Liner leak currents were removed using the P/N method.
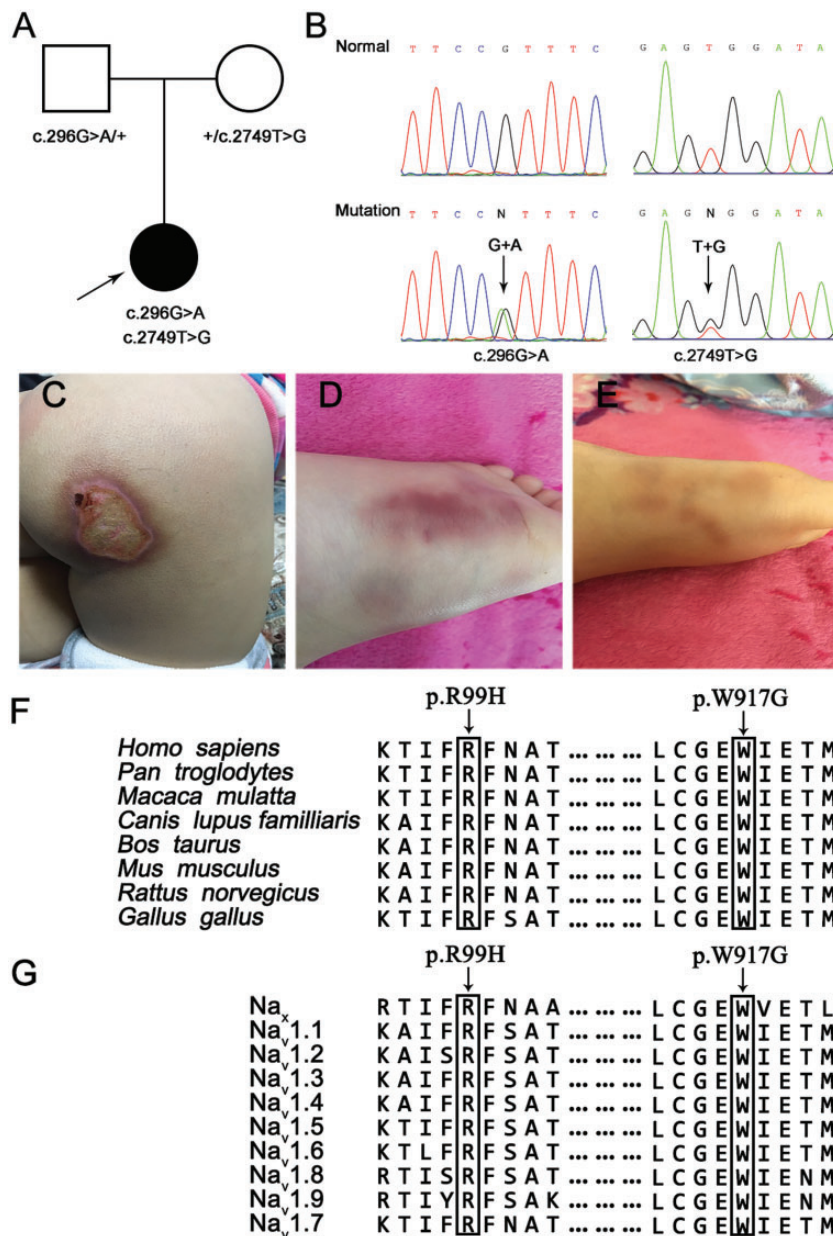
Figure 1. Novel compound heterozygous *SCN9A* mutations identified and the images of damaged tissues in the proband with CIP and anosmia. (a) Family pedigree. The proband is indicated by an arrow. (b) DNA sequence electropherograms demonstrating c.296G>A (p.Arg99His) and c.2749T>G (p.Trp917Gly) mutations in the proband. (c) Burns on the buttock caused by a pressure cooker. (d and e) Injured foot due to bike accident. (f and g) Conservation of residues Arg99 and Trp917 among different species (from *G. gallus* to *H. sapiens*) and sodium channel subtypes (Nav1.1 to Nav1.9 and Nax) in human.

Current–voltage (I–V) relationship was assessed in the potential range from -90 mV to $+45$ mV in 5 mV increments, and current density was calculated by normalizing maximal peak currents to cell capacitance. Peak inward currents obtained from the activation protocol were converted to conductance using the equation: $G = I/(V_m - V_{rev})$, where G is conductance, I is peak inward current, V_m is potential used to elicit the response, and V_{rev} is reversal potential from sodium channel. Conductance data were normalized to the maximum conductance value and fitted with a Boltzmann equation: $G = G_{max} + (G_{min} - G_{max})/(1 + \exp[V_m - V_{1/2}]/k])$, where $V1/2$ is the midpoint of activation and k is the slope factor.

Steady-state fast inactivation was evaluated with a series of 500 ms prepulse (-140 mV to -10 mV in

10 mV increments) followed by a 40 ms step depolarization to −10mV, and the acquired peak inward currents were normalized to the maximum current amplitude.

In the study, data were acquired at a rate of 50 kHz and filtered through a low-pass Bessel filter setting of 10 kHz, and all recordings of all constructs began 5 min after achieving whole-cell configuration. The cells with 10% or greater than peak current and cells with voltage errors >3 mV were excluded from analysis. Finally, the data were analyzed using Clampfit (Molecular Devices), SPSS software (version 22), and Origin 8 (OriginLab).

Reverse transcription-PCR. Total RNA was isolated from transfected HEK293 cells using RNAiso Plus (TaKaRa), and 2 μg RNA was reverse-transcribed into cDNA using Revert Aid Reverse Transcriptase (Thermo Fisher Scientific) according to the manufacturer's instructions. Semi-quantitative PCR was performed with the same amount of template cDNA using the following primers:

SCN9A: 5′-GGTTTCAGCACAGATTCAGGTC-3′ (forward) and

5′-CCAGCTGAAAGTGTCAAAGCTC-3′ (reverse), amplicon size 102 bp;

GAPDH: 5′-AGCCACATCGCTCAGACAC-3′ (forward) and 5′-GCCCAATACGACCAAATCC-3′ (reverse), amplicon size 66 bp.

Thermal cycling conditions were polymerase activation at 95°C for 5 min, and 25 cycles of denaturation at 95°C for 15 s, annealing at 60°C for 30 s, and extension at 60°C for 12 s. The expression level of the *SCN9A* mRNA was normalized to that of *GAPDH* mRNA.

Western blotting

Transfected cells were lysed with lysis buffer containing 20 mM Tris (pH 7.5), 150 mM NaCl, 1% TritonX-100, protease inhibitors (Beyotime Biotechnology), and SIGMAFAST™ Protease Inhibitor cocktail. After incubation for 30 min on ice, cell debris was removed by centrifugation at 12,000 ×g for 10 min at 4°C, and protein concentration was estimated using the Bradford protein assay kit (Beyotime Biotechnology) to ensure equal protein loading. Proteins were separated by electrophoresis on 10% sodium dodecyl sulfate polyacrylamide gels, transferred to a 0.45 μm nitrocellulose membrane (Merck Millipore) and blotted with Nav1.7 rabbit polyclonal antibodies (1:200, Alomone Labs). Positive signals were quantified using ImageJ (v1.50, NIH) and normalized to those of WT Nav1.7 protein levels.

Immunofluorescence staining

Transfected HEK293 cells were fixed with 4% paraformaldehyde for 20 min, permeabilized with 0.5% Triton™ X-100 for 15 min, and blocked with 5% BSA for 30 min at room temperature. Cells were incubated with Nav1.7 polyclonal antibodies (1:200) overnight at 4°C and then incubated with secondary Alexa Fluor 594 labeled anti rabbit IgG (1:500, Life Technologies) for 90 min at 37°C. After that, cell nuclei were stained with DAPI (4′,6-diamidino-2-phenylindole). Images were captured at ×60 magnification using an OLYMPUS FV1000 confocal microscope system. To quantify the subcellular distribution of Nav1.7, fluorescence intensity at the entire cell area was measured with the ROI Manager using ImageJ software, and at least 100 transfected cells were analyzed for each construct.

Statistics

Results are presented as the means ± standard error of the mean (SEM) and compared by independent t-test or one-way analysis of variance to evaluate the significance of differences. Statistical significance was assumed for $P < 0.05$.

Results

Clinical phenotypes of the proband

In the investigated Chinese family, the proband was a 2.5-year-old girl inability to experience pain. She was the only daughter of non-consanguineous parents (Figure 1 (a)) who were normal during pregnancy and childbirth. There was no history of neurological disease in the family. When she was 5-month-old, she often bit her fingers without any signs of unpleasant sensation, later, her parents started to be concerned with her inability to experience pain because she showed no response to injuries of the tongue and lips caused by self-mutilations during teething. She regularly touched her eyes and frequently bruised her body without crying. When she was 26-month-old, her right gluteal region was burned by a pressure cooker and her foot was injured by a bike (Figure 1(c) to (e)), but she did not cry or show displeasure. The proband did not feel pain due to extreme heat or cold, although she could distinguish hot or cold sensations. Fortunately, the proband did not have fractures or dislocation owing to careful supervision of her parents. The proband had impaired sense of smell as she could not distinguish smells of water, alcohol, or white vinegar. There was no obvious autonomic dysfunction, because the blood pressure, sweating, and temperature regulations were normal and the deep reflexes existed. The intelligence level was recognized as average by a pediatrician. There was no obvious abnormality in

electromyography and coronal magnetic resonance imaging. Based on symptomatology, the patient was diagnosed with CIP and anosmia.

Identification of novel SCN9A mutations

The compound heterozygous missense mutations in *SCN9A* were identified: c.296G>C in exon 3 and c.2749T>G in exon 16 inherited from her father and mother, respectively (Figure 1(b)). Genotyping of *SCN9A* mutations in healthy individual using ligase detection reactions (LDRs) by Shanghai BioWing Applied Biotechnology Company (http://www.biowing. com.cn/), we found that these mutations were absent in 500 pairs of unrelated Chinese Han control chromosomes. In addition, neither of these mutations is listed in databases 1000 Genomes Browser (http://www. internationalgenome.org/1000-genomes-browsers), dbSNP (https://www.ncbi.nlm.nih.gov/projects/SNP/), and ExAC Browser (http://exac.broadinstitute.org).

The two Nav1.7 mutations were predicted to result in amino acid substitutions p.Arg99His in the N-terminus and p.Trp917Gly in domain II P-loop. Multiple amino acid sequence alignment showed that residues Arg99 and Trp917 in Nav1.7 were highly conserved among different species (from *Gallus gallus* to *Homo sapiens*) and sodium channel subtypes (Nav1.1 to Nav1.9 and Nax) in human (Figure 1(f) and (g)). The p.Arg99His and p.Trp917Gly mutations were predicted to be deleterious by PolyPhen-2 (scores 0.953 and 1.000, respectively) and sorting intolerant from tolerant (score 0.00 for both).

Electrophysiological properties of mutant Nav1.7 channels

To address the genotype and clinical phenotype correlations in the proband, we investigated the effect of the mutations on the electrophysiological properties of Nav1.7 by performing whole-cell patch-clamp recordings in HEK293 cells expressing WT and mutant Nav1.7 channels. Representative inward sodium channel traces of WT, p.Arg99His, and p.Trp917Gly Nav1.7 are shown in Figure 2(a) to (c). The results indicated that the average peak current density of p.Arg99His channels was only half of that of WT channels (-51.14 ± 8.02 pA/pF vs. -100.98 ± 13.62 pA/pF, respectively), whereas p.Trp917Gly mutation almost abolished the Nav1.7 current (-10.96 ± 1.84 pA/pF; n = 12) (Figure 2 (d) and (e)). However, the voltage-dependent activation of p.Arg99His channels ($V1/2 = -31.86 \pm 1.48$ mV, n = 17) described by the Boltzmann function was only slightly depolarized ($\sim$1.85 mV) compared with that of WT channels ($V1/2 = -33.71 \pm 1.77$ mV, n = 24) and no difference in the slope factor was detected (6.07 ± 0.85 mV for WT and 5.89 ± 0.70 mV for p.Arg99His).

Similarly, no significant difference was observed in the time interval from pulse onset to maximum inward current (time to peak) for voltages between -60 mV and $+20$ mV. Analysis of the steady-state fast inactivation properties showed that p.Arg99His channels exhibited a slight hyperpolarizing shift by -2 mV (-83.98 ± 1.82 mV for WT and -85.43 ± 1.59 mV for p.Arg99His), which did not reach statistical significance (Figure 2(f) to (h)).

Expression of mutant Nav1.7 channels

To determine the expression of Nav1.7, we examined the total Nav1.7 protein levels in HEK293 cells expressing WT and mutant Nav1.7 by Western blotting and immunofluorescence staining. The results of Western blotting showed that the expression of p.Arg99His Nav1.7 protein was significantly reduced to 51% ($P < 0.001$), whereas no difference was observed for p.Trp917Gly Nav1.7 protein compared with WT (Figure 3(a) and (b)), although both mutations showed no change in Nav1.7 mRNA levels (data not shown). Furthermore, the p.Arg99His channel showed lower Nav1.7-specific fluorescence and reduced to $\sim$43% when compared with WT channels, whereas p.Trp917Gly showed the same (WT: 100 ± 3.91%, n = 113; p. Arg99His: 43 ± 3.08%, n = 109, $P < 0.001$; p.Trp917Gly: 99.3 ± 4.09%, n = 114, $P > 0.05$) (Figure 3(c) and (d)).

Discussion

In this study, we identified two novel compound heterozygous missense mutations in *SCN9A* (c.296G>A, p.Arg99His and c.2749T>G, p.Trp917Gly) in the proband suffering from CIP and impaired sense of smell. These mutations were located in the conserved N-terminal region and domain II P-loop of Nav1.7, respectively (Figure S1). Evaluation of the electrophysiological effect exerted by the two mutations revealed that p.Arg99His significantly decreased surface charge density, and p.Trp917Gly almost abolished the sodium current. In addition, p.Arg99His significantly reduced Nav1.7 expression, whereas p.Trp917Gly showed no effect on Nav1.7 protein levels.

Previous studies indicated that the loss of Nav1.7 function in CIP patients was mostly caused by frameshift, nonsense, and splicing mutations in *SCN9A* (Figure S1), which resulted in non-functional and truncated Nav1.7 proteins. Given that Nav1.7 is essential for signal pathways in nociceptive and olfactory sensory neurons,[7,8] the truncating Nav1.7 completely abolishes its function as a voltage-gated sodium channel in nociceptive neurons[9–11] and eliminates presynaptic electrical stimulation, failing to transmit odorant signaling to the olfactory bulb;[8,12] therefore, the phenotypes of
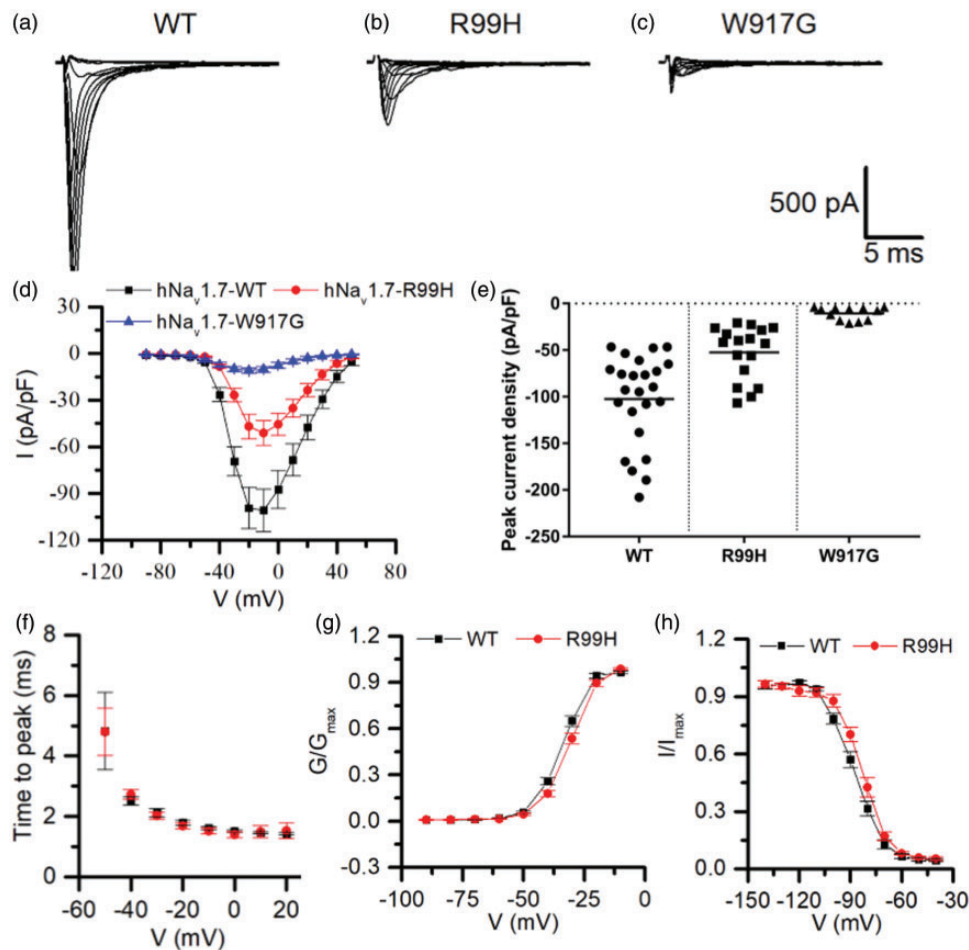
Figure 2. Biophysical characterization of WT and mutant Nav1.7 channels in HEK293 cells. (a–c) Representative inward current traces recorded from HEK293 cells expressing WT, mutant p.Arg99His, and p.Trp917Gly Nav1.7 channels, respectively. (d) Current–voltage relationship of WT and mutant p.Arg99His and p.Trp917Gly channels. Peak current density normalized to membrane capacitance is presented as the mean ± SEM. (e) The scatter plot of peak Nav1.7 current density. (f) Time-to-peak calculated from pulse onset to maximum peak inward current for WT and p.Arg99His mutant channels in the interval between −60 mV to 20 mV. (g) Relative conductance–voltage relationship for WT and p.Arg99His channels. (h) Steady-state fast inactivation for the WT channel and the p.Arg99His mutant channel.

pain-insensitive and anosmia in CIP patients seemed well explained. However, in this study, we identified two novel missense mutations in a patient with CIP and impaired sense of smell, one of which (p.Arg99His) decreased, but not abolished current density and then still retained partial Nav1.7 function. The unexpected electrophysiological and clinical phenotypic relationship in our patient was challenge the previous findings "Nav1.7 total loss-of-function leads to painlessness."[9–11]

Residue Arg99 mapped to the N-terminal region of Nav1.7 is highly conserved among different subtypes of human voltage-gated sodium channels. Coincidentally, mutations in this site of the Nav1.4 and Nav1.5 channels have been associated with pathological conditions. Thus, p.Arg104His in Nav1.4 was linked to congenital myopathy and p.Arg104Trp/Gln in Nav1.5 was reported to cause Brugada syndrome and the disease of long QT

syndrome, respectively, due to loss-of-function and probably significant protein degradation.[13–15] Here, electrophysiological data indicated that p.Arg99His resulted in a significant reduction of peak current, although channel activation and steady-state inactivation did not significantly differ from those of WT Nav1.7. Furthermore, we analyzed the expression of the WT and mutant Nav1.7 channels in transfected HEK293 cells by semi-quantitative PCR, Western blotting, and immunostaining. The results showed that although the Nav1.7 mRNA expression was not affected by the mutations, protein expression of the p.Arg99His mutant was significantly decreased. We speculated that these effects may be due to the degradation of the misfolded Nav1.7 protein. These data further confirmed the key role of the conserved Arg residue in maintaining the stability of the sodium channel Nav1.7.
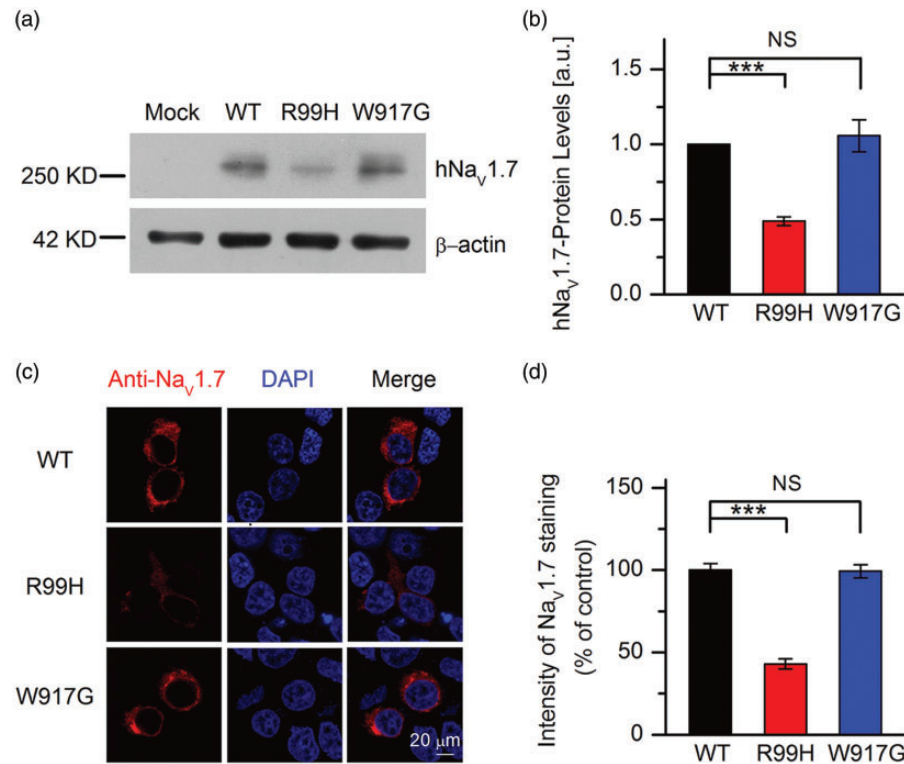
Figure 3. The expression and subcellular location of WT and mutant Nav1.7 channels in HEK293 cells. (a) Expression of WT and mutant Nav1.7 channels in HEK293 cells analyzed by Western blotting. (b) Quantitative analysis based on three independent experiments, data are presented as the mean ± SEM (***$P < 0.001$; NS: not significant). (c) Immunostaining analysis of HEK293 cells expressing WT or mutant Nav1.7 sodium channels. Representative confocal microscopy images show membrane localization of Nav1.7 sodium channels. Scale bars: 20 μm. (d) Fluorescence intensity of mutant Nav1.7 channels relative to that of the WT Nav1.7 channels was quantified. Data are presented as the mean ± SEM. ***$P < 0.001$. WT: wild-type; NS: not significant.

The S5–S6 region of domain II in Nav1.7 (Figure S2 (a) and (b)) contributes to a quarter in formation of the sodium channel selectivity filter (also called the pore region) and is highly evolutionary conserved among the four homologous repeats of sodium and calcium channels from bacteria to mammal (Figure S2(c)). The selectivity filter can be divided into three regions: S5-P, P loop, and P-S6[16,17] (Figure S2(b)). The p.Arg896Gln mutation detected in one CIP patient is located in the S5-P outside the mouth of the pore and is reported to abolish the channel current.[11] The Trp917 residue mutated in our patient is mapped to the P loop inside the mouth of the pore selectivity filter where it plays an important role in filtering sodium ions.[17] Trp contains an aromatic ring and is capable of hydrogen bonding with adjacent amino acids via the side chain indole nitrogen to refine and stabilize the selectivity filter (Figure S2 (d)),[18,19] otherwise, the disruption of H-bonding or selectivity filter sequence dramatically altered the channel selectivity profiles.[20,21] In our study, the p.Trp917Gly substitution completely abolished Nav1.7 function, although the expression was not affected. We suggest that p.Trp917Gly mutation destroyed hydrogen bonding

and weakened Nav1.7 gating and sodium permeation. These data confirmed that the selectivity filter can modulate sodium current and that Trp917 residue plays a significant role in maintaining the physiological function of sodium channel Nav1.7.

The previous studies showed that current threshold for action potential generation in dorsal root ganglion neurons is regulated by Nav1.7 conductance in a remarkably linear manner.[22,23] Neuron simulations show subthreshold membrane potential oscillations in the interval between action potentials when the action potential frequency is low. The expression of Nav1.7 increases the amplitude of subthreshold oscillations and decreases the interspike interval, several picoamperes of Nav1.7 current would be expected to depolarize membrane potential by a few millivolts, opening even more sodium channels and allowing more depolarization in a positive-feedback manner, which provide a mechanistic basis for reduced current threshold and enhanced action potential firing probability. Here, electrophysiological results showed that compared with WT, the peak current following activation was reduced significantly in Nav1.7 mutations, resulting in positive-feedback manner

was disappearance and further neuronal excitability was reduced; thus, the patient showed insensitivity to pain. Our findings are similar to those reported previously in two families who had p.Trp1775Arg/p.Leu1831X and p.Leu1831X/p.Ala1236Glu mutations, respectively, which did not fully eliminate Nav1.7 function but resulted in complete insensitivity to pain.[24] Interestingly, Staud et al. described a patient with "partial" CIP who carried a missense mutation p.Cys1719Arg and a 1-bp splice donor deletion, which led the authors to speculate that a partial loss of pain perception may be caused by diminished Nav1.7 function.[25] Although more evidence is still needed, it is worth noting that the degree of pain insensitivity may be defined by the number of functional Nav1.7, which may influence the analgesic efficacy of a Nav1.7-selective inhibitor.

Conclusions

In summary, we identified two novel loss-of-function missense mutations in *SCN9A* (c.296G>A, p.Arg99His and c.2749T>G, p.Trp917Gly) as the cause of CIP with anosmia in a Chinese Han girl. Our findings are consistent with the earlier Emery et al.'s publication, and the unexpected relationship between electrophysiological characterization and clinical phenotype resulted from *SCN9A* mutations shown in the patient should be emphasized highly. In addition, the findings expand the spectrum of *SCN9A* mutation underlying CIP and confirm the crucial role of the N-terminal region and domain II P-loop in function of Nav1.7, thus promoting the development of Nav1.7-targeting analgesics.

Author Contributions

XZ and JYL designed and supervised the project, analyzed the data, and edited the manuscript. JS and LL designed the experiments, carried out the molecular cloning, and wrote manuscript. LL carried out Western blotting, immunofluorescence and microscopic analyses. LY conducted the electrophysiological experiments. GD collected and analyzed the data. TM conducted the cell culture and transfection. JS, NL, and YL recruited subjects, and collected blood samples. JY analyzed the data and edited manuscript. All authors reviewed the article, and approved the article for submission.

Declaration of Conflicting Interests

The author(s) declared no potential conflicts of interest with respect to the research, authorship, and/or publication of this article.

ORCID iD

Xianwei Zhang https://orcid.org/0000-0003-0907-7621

Supplemental Material

Supplemental material for this article is available online.

References

1. Waxman SG, Merkies IS, Gerrits MM, Dib-Hajj SD, Lauria G, Cox JJ, Wood JN, Woods CG, Drenth JP, Faber CG. Sodium channel genes in pain-related disorders: phenotype-genotype associations and recommendations for clinical use. *Lancet Neurol* 2014; 13: 1152–1160.
2. Catterall WA. From ionic currents to molecular mechanisms: the structure and function of voltage-gated sodium channels. *Neuron* 2000; 26: 13–25.
3. Hinard V, Britan A, Schaeffer M, Zahn-Zabal M, Thomet U, Rougier JS, Bairoch A, Abriel H, Gaudet P. Annotation of functional impact of voltage-gated sodium channel mutations. *Hum Mutat* 2017; 38: 485–493.
4. Habib AM, Wood JN, Cox JJ. Sodium channels and pain. *Handb Exp Pharmacol* 2015; 227: 39–56.
5. Vetter I, Deuis JR, Mueller A, Israel MR, Starobova H, Zhang A, Rash LD, Mobli M. NaV1.7 as a pain target - From gene to pharmacology. *Pharmacol Ther* 2017; 172: 73–100.
6. Klugbauer N, Lacinova L, Flockerzi V, Hofmann F. Structure and functional expression of a new member of the tetrodotoxin-sensitive voltage-activated sodium channel family from human neuroendocrine cells. *Embo J* 1995; 14: 1084–1090.
7. Minett MS, Falk S, Santana-Varela S, Bogdanov YD, Nassar MA, Heegaard AM, Wood JN. Pain without nociceptors? Nav1.7-independent pain mechanisms. *Cell Rep* 2014; 6: 301–312.
8. Weiss J, Pyrski M, Jacobi E, Bufe B, Willnecker V, Schick B, Zizzari P, Gossage SJ, Greer CA, Leinders-Zufall T, Woods CG, Wood JN, Zufall F. Loss-of-function mutations in sodium channel Nav1.7 cause anosmia. *Nature* 2011; 472: 186–190.
9. Ahmad S, Dahllund L, Eriksson AB, Hellgren D, Karlsson U, Lund P-E, Meijer IA, Meury L, Mills T, Moody A, Morinville A, Morten J, O'donnell D, Raynoschek C, Salter H, Rouleau GA, Krupp JJ. A stop codon mutation in SCN9A causes lack of pain sensation. *Hum Mol Genet* 2007; 16: 2114–2121.

10. Cox JJ, Reimann F, Nicholas AK, Thornton G, Roberts E, Springell K, Karbani G, Jafri H, Mannan J, Raashid Y, Al-Gazali L, Hamamy H, Valente EM, Gorman S, Williams R, Cox JJ, Reimann F, Nicholas AK, Thornton G, Roberts E, Springell K, Karbani G, Jafri H, Mannan J, Raashid Y, Al-Gazali L, Hamamy H, Valente EM, Gorman S, Williams R, McHale DP, Wood JN, Gribble FM, Woods CG. An SCN9A channelopathy causes congenital inability to experience pain. *Nature* 2006; 444: 894–898.

11. Cox JJ, Sheynin J, Shorer Z, Reimann F, Nicholas AK, Zubovic L, Baralle M, Wraige E, Manor E, Levy J, Woods CG, Parvari R. Congenital insensitivity to pain: novel SCN9A missense and in-frame deletion mutations. *Hum Mutat* 2010; 31: E1670–1686.

12. Ahn H-S, Black JA, Zhao P, Tyrrell L, Waxman SG, Dib-Hajj SD. Dib-Hajj SD. Nav1.7 is the predominant sodium channel in rodent olfactory sensory neurons. *Mol Pain* 2011; 7: 32.

13. Clatot J, Ziyadeh-Isleem A, Maugenre S, Denjoy I, Liu H, Dilanian G, Hatem SN, Deschenes I, Coulombe A, Guicheney P, Neyroud N. Dominant-negative effect of SCN5A N-terminal mutations through the interaction of Na(v)1.5 alpha-subunits. *Cardiovasc Res* 2012; 96: 53–63.

14. Gutter C, Benndorf K, Zimmer T. Characterization of N-terminally mutated cardiac Na(+) channels associated with long QT syndrome 3 and Brugada syndrome. *Front Physiol* 2013; 4: 153.

15. Zaharieva IT, Thor MG, Oates EC, van Karnebeek C, Hendson G, Blom E, Witting N, Rasmussen M, Gabbett MT, Ravenscroft G, Sframeli M, Suetterlin K, Sarkozy A, D'Argenzio L, Hartley L, Matthews E, Pitt M, Vissing J, Ballegaard M, Krarup C, Slørdahl A, Halvorsen H, Ye XC, Zhang L-H, Løkken N, Werlauff U, Abdelsayed M, Davis MR, Feng L, Phadke R, Sewry CA, Morgan JE, Laing NG, Vallance H, Ruben P, Hanna MG, Lewis S, Kamsteeg E-J, Männikkö R, Muntoni F. Loss-of-function mutations in SCN4A cause severe foetal hypokinesia or 'classical' congenital myopathy. *Brain* 2016; 139: 674–691.

16. Fozzard HA, Hanck DA. Structure and function of voltage-dependent sodium channels: comparison of brain II and cardiac isoforms. *Physiol Rev* 1996; 76: 887–926.

17. Li RA, Ennis IL, Xue T, Nguyen HM, Tomaselli GF, Goldin AL, Marban E. Molecular basis of isoform-specific micro-conotoxin block of cardiac, skeletal muscle, and brain Na+ channels. *J Biol Chem* 2003; 278: 8717–8724.

18. Payandeh J, Gamal El-Din TM, Scheuer T, Zheng N, Catterall WA. Crystal structure of a voltage-gated sodium channel in two potentially inactivated states. *Nature* 2012; 486: 135–139.

19. Payandeh J, Scheuer T, Zheng N, Catterall WA. The crystal structure of a voltage-gated sodium channel. *Nature* 2011; 475: 353–358.

20. Naylor CE, Bagneris C, DeCaen PG, Sula A, Scaglione A, Clapham DE, Wallace BA. Molecular basis of ion permeability in a voltage-gated sodium channel. *Embo J* 2016; 35: 820–830.

21. Pless SA, Elstone FD, Niciforovic AP, Galpin JD, Yang R, Kurata HT, Ahern CA. Asymmetric functional contributions of acidic and aromatic side chains in sodium channel voltage-sensor domains. *J Gen Physiol* 2014; 143: 645–656.

22. Choi JS, Waxman SG. Physiological interactions between Nav1.7 and Nav1.8 sodium channels: a computer simulation study. *J Neurophysiol* 2011; 106: 3173–3184.

23. Vasylyev DV, Han C, Zhao P, Dib-Hajj S, Waxman SG. Dynamic-clamp analysis of wild-type hNaV1.7 and erythromelalgia mutant channel L858H. *J Neurophysiol* 2014; 111: 1429–1443.

24. Emery EC, Habib AM, Cox JJ, Nicholas AK, Gribble FM, Woods CG, Reimann F. Novel SCN9A mutations underlying extreme pain phenotypes: unexpected electrophysiological and clinical phenotype correlations. *J Neurosci* 2015; 35: 7674–7681.

25. Staud R, Price DD, Janicke D, Andrade E, Hadjipanayis AG, Eaton WT, Kaplan L, Wallace MR. Two novel mutations of SCN9A (Nav1.7) are associated with partial congenital insensitivity to pain. *Eur J Pain*. 2011; 15: 223–230.